# Electronic Supplementary Information

## Experimental Section

**Materials:** The CNT was purchased from Chengdu Kelong Chemical Reagent Factory. Sodium salicylate ($C_7H_5O_3Na$), sodium hydroxide (NaOH), lithium perchlorate ($LiClO_4$), ammonium chloride ($NH_4Cl$), sodium nitroferricyanide ($C_5FeN_6Na_2O$), *p*-dimethylaminobenzaldehyde (*p*-$C_9H_{11}NO$), and N-[Tris(hydroxymethyl)metyl]-3-aminopropanesulfo (TAPS) were obtained from Sigma-Aldrich Chemical Reagent Co., Ltd. Hydrochloric acid (HCl), nitric acid ($HNO_3$), sodium hypochlorite (NaClO), Nafion (5 wt%) solution, hydrazine hydrate ($N_2H_4{\cdot}H_2O$), and ethanol were obtained from Aladdin Ltd. (Shanghai, China). Ultrapure water used throughout all experiments was purified through a Millipore system.

**Preparation of O-CNT$_x$:** The pre-determined quantities of CNT and $HNO_3$ were kept at 80 $^oC$ for 12, 24, 36, and 48 h. Then, the slurry was taken out, cooled, centrifuged, and washed with water and ethanol several times until the pH was neutral. Finally, the samples (O-CNT$_1$, O-CNT, O-CNT$_3$, and O-CNT$_4$) were dried at 60 °C in a vacuum oven overnight.

**Characterizations:** XRD patterns were obtained from a Shimazu XRD-6100 diffractometer with Cu Kα radiation (40 kV, 30 mA) of wavelength 0.154 nm (Japan). Raman spectra were recorded from 300 to 600 $cm^{-1}$ with a Horiba LabRAm HR Evolution spectrometer. SEM images were collected from the tungsten lamp-equipped SU3500 SEM at an accelerating voltage of 20 kV (HITACHI, Japan). TEM images were obtained from a Zeiss Libra 200FE transmission electron microscope operated at 200 kV. XPS measurements were performed on an ESCALABMK II X-ray photoelectron spectrometer using Mg as the exciting source. The absorbance data of spectrophotometer were measured on SHIMADZU UV-2700 ultraviolet-visible

(UV-Vis) spectrophotometer. $^1$H nuclear magnetic resonance (NMR) spectra were collected on a super-conducting-magnet NMR spectrometer (Bruker AVANCE III HD 500 MHz) and dimethyl sulphoxide was used as an internal to calibrate the chemical shifts in the spectra.

**Electrochemical measurements:** $N_2$ reduction experiments were carried out in a two-compartment cell under ambient condition, which is separated by the Nafion 117 membrane. All experiments were carried out at room temperature (25 °C). A carbon paper electrode loaded with the O-CNT was used as the working electrode, a graphite rod as the counter electrode and Ag/AgCl electrode as the reference. The potentials reported in this work were converted to RHE scale via calibration with the following equation: E (*vs*. RHE) =E (*vs*. Ag/AgCl) + 0.197 + 0.059 × pH. The catalyst ink was prepared by blending 5 mg catalyst powder with 20 μL Nafion binder (5 wt%), 490 μL ultrapure water and 490 μL ethanol in an ultrasonic bath for 1 h. For NRR tests, the $LiClO_4$ electrolyte (0.1 M, pH = 7) was bubbled with $N_2$ for 30 min before measurement.

**Determination of $NH_3$:** Concentration of produced $NH_3$ was spectrophotometrically determined by the indophenol blue method.[1] In detail, 4 mL electrolyte was obatined from the cathodic chamber and mixed with 50 μL oxidizing solution containing NaClO (ρCl = 4 ~ 4.9) and NaOH (0.75 M), 500 μL coloring solution containing 0.4 M $C_7H_5O_3Na$ and 0.32 M NaOH, and 50 μL catalyst solution (1 wt% $C_5FeN_6Na_2O$) for 1 h. The concentration of indophenol blue was determined using the absorbance at awavelength of 655 nm. The concentration-absorbance curve was calibrated using standard ammonia chloride solution with a serious of concentrations. The fitting curve ($y = 0.6105x + 0.0115$, $R^2 = 0.997$) shows good linear relation of absorbance value with $NH_4Cl$ concentration.

**Determination of $N_2H_4$:** The $N_2H_4$ present in the electrolyte was determined by the method of Watt and Chrisp.[2] A mixed solution of 5.99 g *p*-$C_9H_{11}NO$, 30 mL HCl and

300 mL ethanol was used as the colour reagent. The calibration curve was achieved based on a series of reference solutions, which was added 5 mL colour reagent and stirred 20 min at room temperature. Moreover, the absorbance of the resulting solution was measured at a wavelength of 455 nm, and the yield of $N_2H_4$ were evaluated from a standard curve using 5 mL residual electrolyte and 5 mL color reagent. Absolute calibration of this method was carried out using the $N_2H_4$ solution as a standard, and the fitting curve showed a good linear relation of absorbance with the $N_2H_4$ concentration ($y = 0.6304x + 0.0291$, $R^2 = 0.999$).

**Calculations of $V_{NH3}$ formation rate and FE:** $V_{NH3}$ was calculated using the following equation:

$$V_{NH3} = [NH_3] \times V / (m_{cat.} \times t)$$

FE was calculated according to following equation:

$$FE = 3 \times 10^{-3} \times F \times [NH_3] \times V / (M_{NH3} \times Q)$$

Where $[NH_3]$ is the measured $NH_3$ concentration (μg $mL^{-1}$); V is the volume of the cathodic reaction electrolyte (mL); $m_{cat.}$ is the catalyst loading quality (mg); t is the reduction reaction time (h); F is the Faraday constant (96485 C $mol^{-1}$); $M_{NH3}$ is relative molecular mass of $NH_3$ (17g $mol^{-1}$); and Q is the quantity of applied electricity (C).

**Theoretical Method:** All density functional theory (DFT) calculations were conducted using Vienna Ab-initio Simulation Package (VASP). The electron exchange was described by employing Perdew-Burke-Ernzerhof (PBE) function and a generalized gradient approximation (GGA). The projector augmented wave (PAW) method was utilized to describe the electron-ion interaction. The kinetic energy cutoff for planewave was chosen as 400 eV. The convergence criteria for the structure

relaxation were set as $10^{-4}$ eV for atomic energy and -0.02 eV $Å^{-1}$ for atomic force, respectively.[3] The Brillioun zone was sampled by a 3 × 3 × 1 k-points grid.

A (6, 0) single wall carbon nanotube was chosen as the pristine CNT. To simulate the O-CNT with different functional group doping, two carbon atoms were removed from the O-CNT to generate defects for the doping of oxygen-containing groups. The oxygen functional groups include single O atom (C-O), hydroxy (OH), carbonyl group (C=O) and carboxyl (COOH). A 20 Å vacuum layer was introduced to avoid the effect of periodicity.

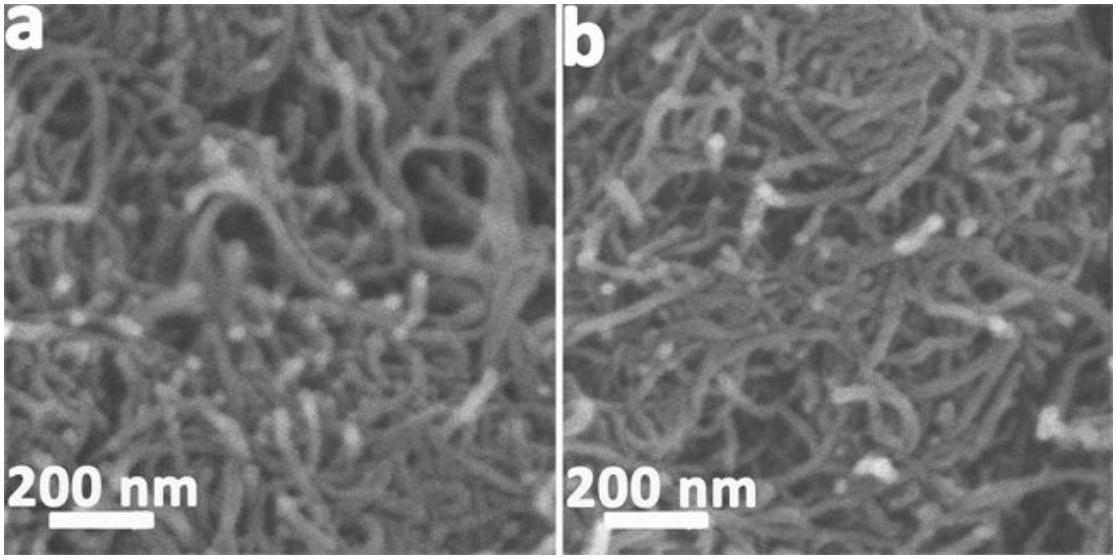


**Fig. S1.** SEM images for O-CNT and CNT.

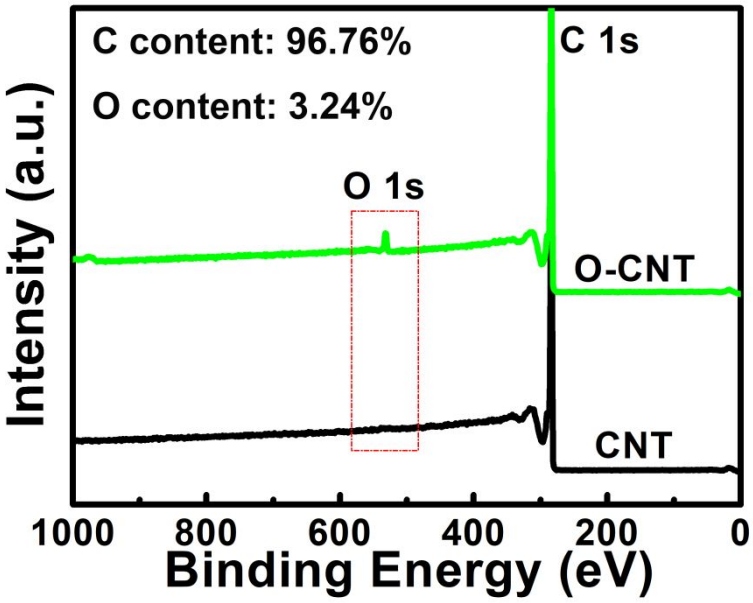


**Fig. S2.** XPS spectra for O-CNT and CNT.

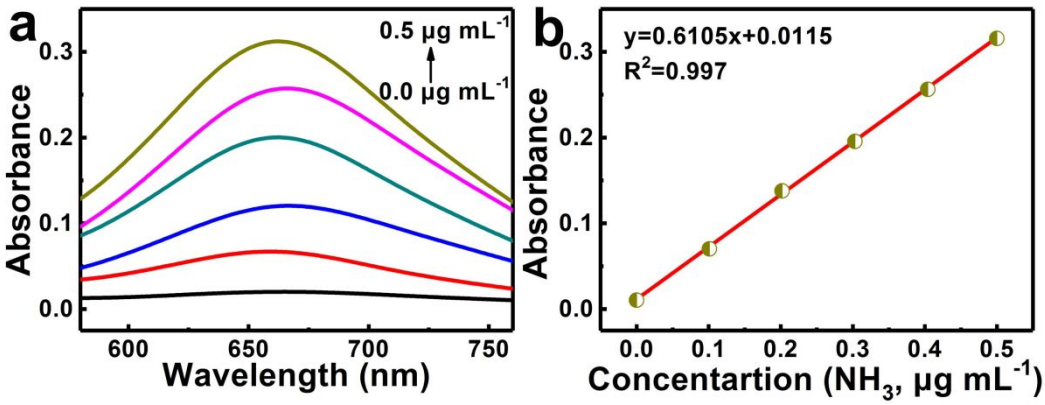


**Fig. S3.** (a) UV-Vis absorption spectra of various $NH_3$ concentrations after incubated for 2 h at room temperature. (b) Calibration curve used for estimation of $NH_3$ concentration.

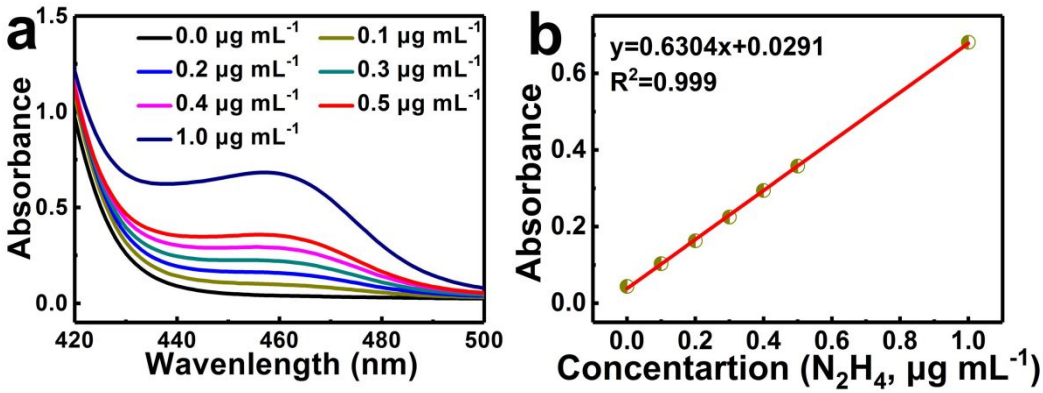


**Fig. S4.** (a) UV-Vis absorption spectra of various $N_2H_4$ concentrations after incubated for 15 min at room temperature. (b) Calibration curve used for estimation of $N_2H_4$ concentration.

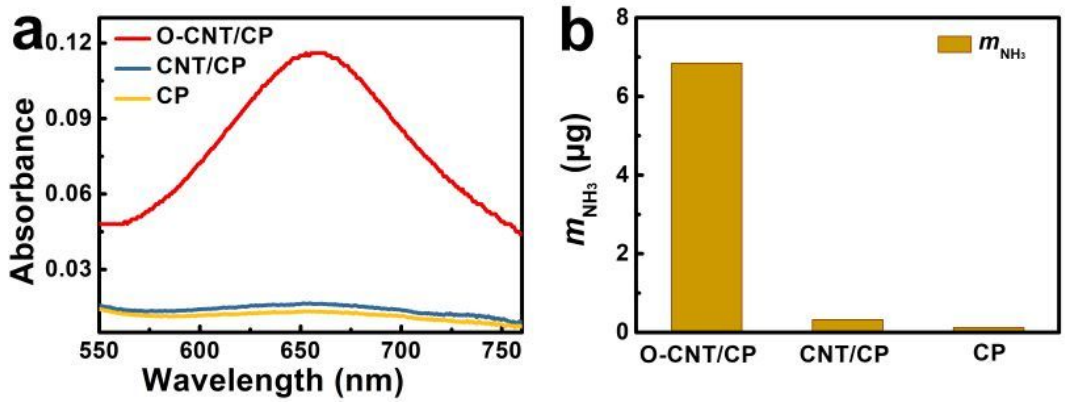


**Fig. S5.** (a) UV–vis absorption spectra of the electrolytes stained with indophenol indicator and (b) $m_{NH3}$ for O-CNT/CP, CNT/CP, and CP after charging at −0.4 V for 2 h.

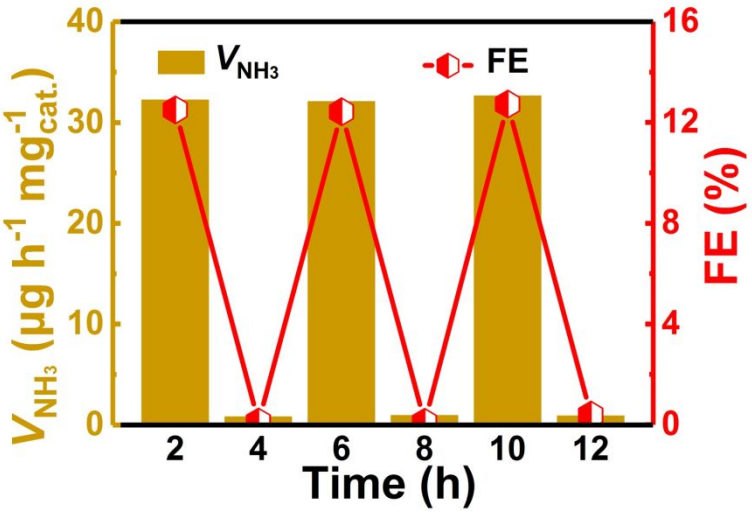


**Fig. S6.** $V_{NH3}$ and corresponding FEs of O-CNT/CP with alternating 2-h cycles between $N_2$- and Ar-saturated electrolytes.

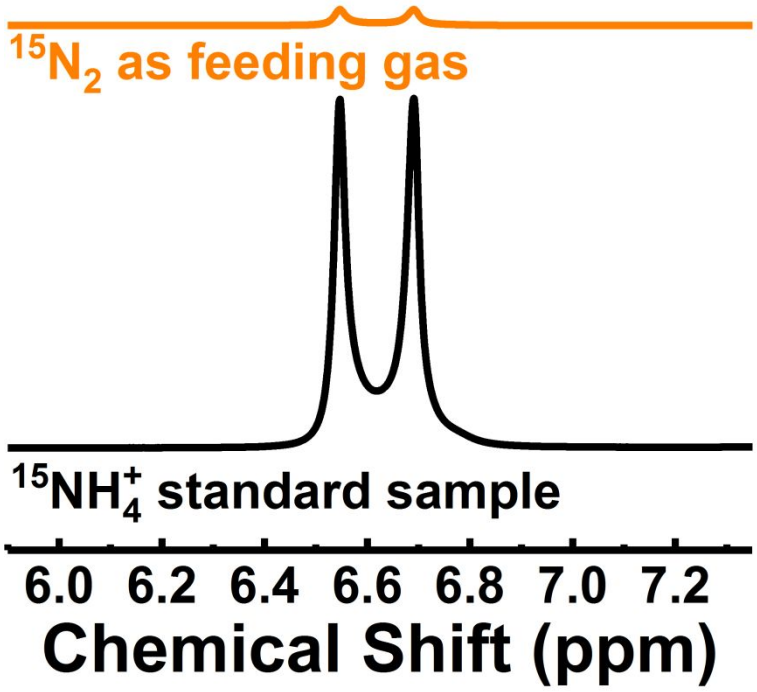


**Fig. S7.** $^{1}H$ NMR spectra of $^{15}NH_4^+$ calibration solution and after electrolysis at the potential of –0.4 V under $^{15}N_2$ atmosphere on the O-CNT/CP electrode.

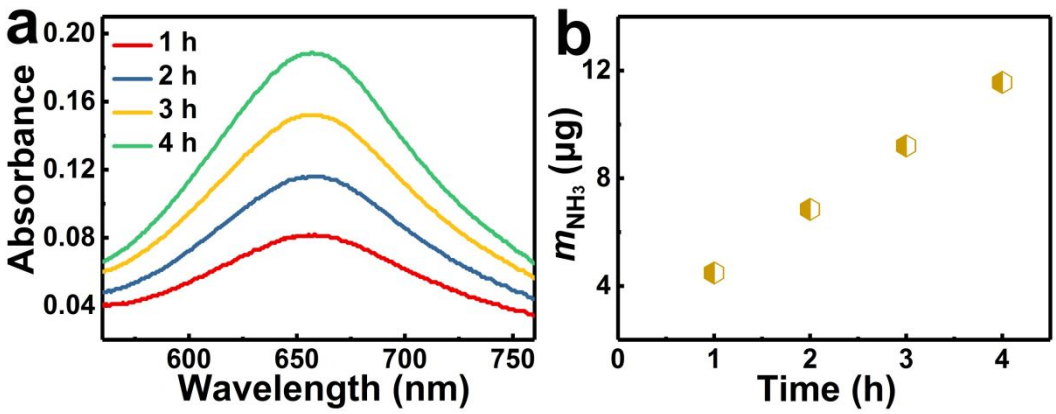


**Fig. S8.** (a) UV-Vis absorption spectra of the electrolytes stained with indophenol indicator after NRR electrolysis at a series of time. (b) $m_{NH3}$ *vs.* time recorded at –0.4 V for O-CNT/CP.

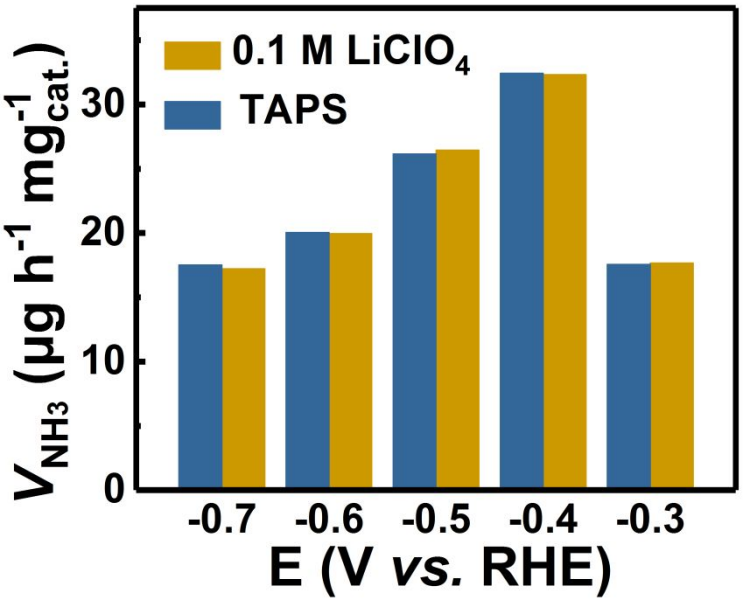


**Fig. S9.** $V_{NH3}$ for O-CNT/CP at a series of potentials in 0.1 M $LiClO_4$ and TAPS.

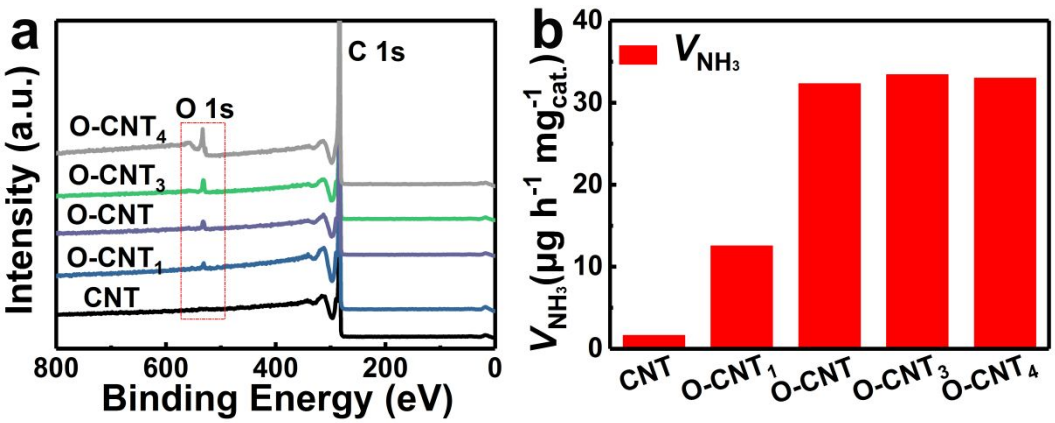


**Fig. S10.** (a) XPS spectra for CNT and O-CNT with diffirent O content.

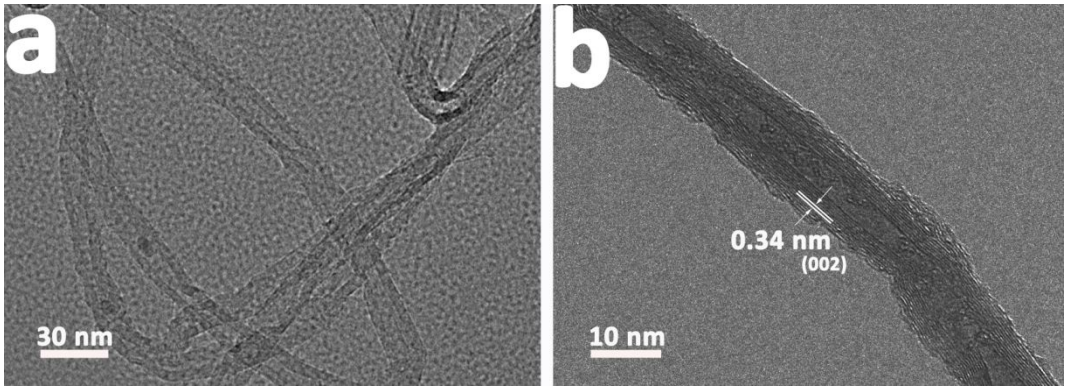


**Fig. S11.** (a) TEM and (b) HRTEM images for post-NRR O-CNT.

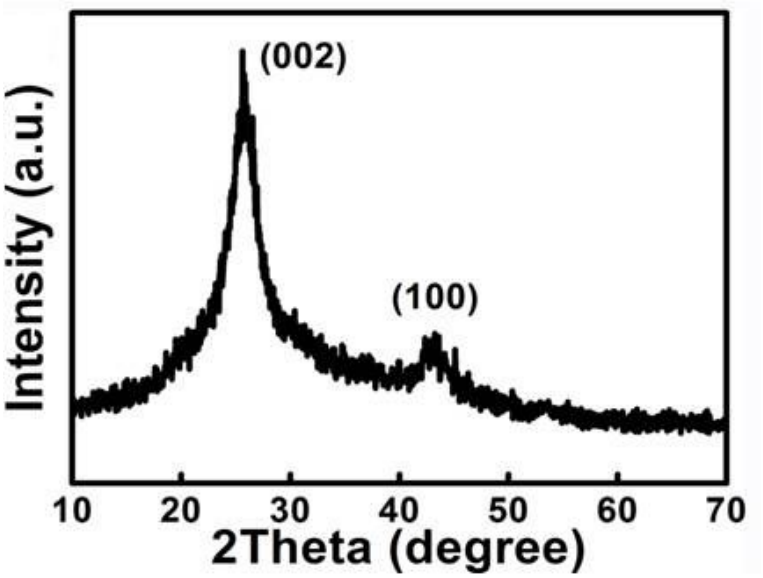


**Fig. S12.** XRD pattern for post-NRR O-CNT.

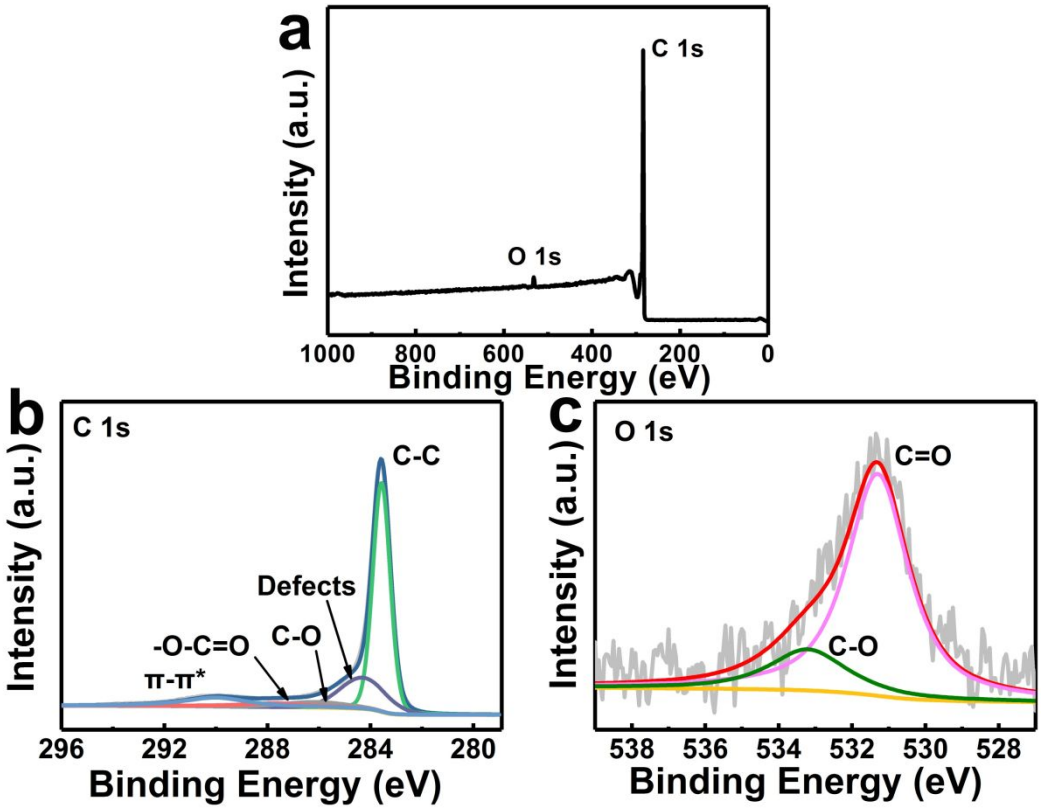


**Fig. S13.** (a) XPS survey spectrum for post-NRR O-CNT. (b) XPS spectra for post-NRR O-CNT in the (b) C 1s and (c) O 1s regions.

**Table S1.** Comparison of the $NH_3$ electrosynthesis activity for O-CNT with other NRR catalysts under ambient conditions.

| Catalyst | $V_{NH3}$ | FE | Ref. |
|---|---|---|---|
| O-CNT/CP | 33.23 μg $h^{-1}$ $mg_{cat.}^{-1}$ | 12.50% | This work |
| $Fe_2O_3$-CNT | $3.58\times10^{-12}$ mol $s^{-1}$ $cm^{-2}$ | 0.15% | 4 |
| γ-$Fe_2O_3$ | 0.21 μg $h^{-1}$ $mg^{-1}_{cat.}$ | 1.9% | 5 |
| $Bi_4V_2O_{11}/CeO_2$ | 23.2 μg $h^{-1}$ $mg^{-1}_{cat.}$ | 10.16% | 6 |
| Au nanorods | 6.04 μg $h^{-1}$ $mg^{-1}_{cat.}$ | 4.00% | 7 |
| α-Au/$CeO_x$-RGO | 8.31 μg $h^{-1}$ $mg^{-1}_{cat.}$ | 10.10% | 8 |
| Mo nanofilm | $3.09\times10^{-11}$ mol $s^{-1}$ $cm^{-2}$ | 0.72% | 9 |
| $MoS_2$ | $8.08\times10^{-11}$ mol $s^{-1}$ $cm^{-2}$ | 1.17% | 10 |
| Ru/C | $3.44\times10^{-12}$ mol $s^{-1}$ $cm^{-2}$ | 0.28% | 11 |
| NPC | 27.2 μg $h^{-1}$ $mg^{-1}_{cat.}$ | 1.42% | 12 |
| ZIF-derived carbon | 57.8 μg $h^{-1}$ $cm^{-2}_{cat.}$ | 10.20% | 13 |
| $MoO_3$ | 29.43 μg $h^{-1}$ $mg_{cat.}^{-1}$ | 1.9% | 14 |
| $Mo_2N$ | 78.4 μg $h^{-1}$ $mg_{cat.}^{-1}$ | 4.5% | 15 |
| MoN | $3.01\times10^{-10}$ mol $s^{-1}$ $cm_{cat.}^{-2}$ | 1.15% | 16 |
| defect-rich $MoS_2$ | 29.28 μg $h^{-1}$ $mg_{cat.}^{-1}$ | 8.34% | 17 |
| TA-reduced Au/$TiO_2$ | 21.4 μg $h^{-1}$ $mg_{cat.}^{-1}$ | 8.11% | 18 |
| $Fe_3O_4$/Ti | $5.6\times10^{-11}$ mol $s^{-1}$ $cm_{cat.}^{-2}$ | 2.6% | 19 |
| $Bi_4V_2O_{11}/CeO_2$ | 23.21 μg $h^{-1}$ $mg_{cat.}^{-1}$ | 10.16% | 20 |
| $TiO_2$ nanosheets | 5.6 μg $h^{-1}$ $cm_{cat.}^{-1}$ | 2.50% | 21 |
| $MoS_2$/CC | 4.94 μg $h^{-1}$ $cm_{cat.}^{-2}$ | 1.17% | 22 |
| Pd/C | 4.5 μg $h^{-1}$ $mg_{cat.}^{-1}$ | 8.2% | 23 |
| $B_4C$ | 26.57 μg $h^{-1}$ $mg_{cat.}^{-1}$ | 15.96% | 24 |

## References


1 D. Zhu, L. Zhang, R. E. Ruther and R. J. Hamers, *Nat. Mater.*, 2013, **12**, 836–841.

2 G. W. Watt and J. D. Chrisp, *Anal. Chem.*, 1952, **24**, 2006–2008.

3 F. Gong, Z. Ding, Y. Fang, C. Tong, D. Xia, Y. Lv, B. Wang, D. V. Papavassiliou, J. Liao and M. Wu, *ACS Appl. Mater. Interfaces*, 2018, **10**, 14614–14621.

4 S. Chen, S. Perathoner, C. Ampelli, C. Mebrahtu, D. Su and G. Centi, *Angew. Chem., Int. Ed.*, 2017, **56**, 2699–2703.

5 J. Kong, A. Lim, C. Yoon, J. H. Jang, H. C. Ham, J. Han, S. Nam, D. Kim, Y. E. Sung, J. Choi and H. S. Park, *ACS Sustainable Chem. Eng.*, 2017, **5**, 10986–10995.

6 C. Lv, C. Yan, G. Chen, Y. Ding, J. Sun, Y. Zhou and G. Yu, *Angew. Chem., Int. Ed.*, 2018, **57**, 6073–6076.

7 D. Bao, Q. Zhang, F. Meng, H. Zhong, M. Shi, Y. Zhang, J. Yan, Q. Jiang and X. Zhang, *Adv. Mater.*, 2017, **29**, 1604799.

8 S. Li, D. Bao, M. Shi, B. Wulan, J. Yan and Q. Jiang, *Adv. Mater.*, 2017, **29**, 1700001.

9 D. Yang, T. Chen and Z. Wang, *J. Mater. Chem. A*, 2017, **5**, 18967–18971.

10 L. Zhang, X. Ji, X. Ren, Y. Ma, X. Shi, A. M. Asiri, L. Chen, B. Tang and X. Sun, *Adv. Mater.*, 2018, **30**, 1800191.

11 V. Kordali, G. Kyriacou and C. Lambrou, *Chem. Commun.*, 2000, **17**, 1673–1674.

12 Y. Liu, Y. Su, X. Quan, X. Fan, S. Chen, H. Yu, H. Zhao, Y. Zhang and J. Zhao, *ACS Catal.*, 2018, **8**, 1186–1191.

13 S. Mukherjee, D. A. Cullen, S. Karakalos, K. Liu, H. Zhang, S. Zhao, H. Xu, K. L. More, G. Wang and G. Wu, *Nano Energy*, 2018, **48**, 217–226.

14 J. Han, X. Ji, X. Ren, G. Cui, L. Li, F. Xie, H. Wang, B. Li and X. Sun, *J. Mater. Chem. A*, 2018, **6**, 12974–12977.

15 X. Ren, G. Cui, L. Chen, F. Xie, Q. Wei, Z. Tian and X. Sun, *Chem. Commun.*, 2018, **54**, 8474–8477.

16 L. Zhang, X. Ji, X. Ren, Y. Luo, X. Shi, A. M. Asiri, B. Zheng and X. Sun, *ACS Sustainable Chem. Eng.*, 2018, **6**, 9550–9554.

17 X. Li, T. Li, Y. Ma, Q. Wei, W. Qiu, H. Guo, X. Shi, P. Zhang, A. M. Asiri, L. Chen, B. Tang and X. Sun, *Adv. Energy Mater.*, 2018, **8**, 1801357.

18 M. Shi, D. Bao, B. Wulan, Y. Li, Y. Zhang, J. Yan and Q. Jiang, *Adv. Mater.*, 2017, **29**, 1606550.

19 Q. Liu, X. Zhang, B. Zhang, Y. Luo, G. Cui, F. Xie and X. Sun, *Nanoscale*, 2018, **10**, 14386–14389.

20 C. Lv, C. Yan, G. Chen, Y. Ding, J. Sun, Y. Zhou and G. Yu, *Angew. Chem., Int. Ed.*, 2018, **57**, 6073–6076.

21 R. Zhang, X. Ren, X. Shi, F. Xie. B. Zheng, X. Guo and X. Sun, *ACS Appl. Mater. Interfaces*, 2018, **10**, 28251–28255.

22 L. Zhang, X. Ji, X. Ren, Y. Ma, X. Shi, Z. Tian, A. M. Asiri, L. Chen, B. Tang and X. Sun, *Adv. Mater.*, 2018, **30**, 1800191.

23 J. Wang, L. Yu, L. Hu, G. Chen, H. Xin and X. Feng, *Nat. Commun.*, 2018, **9**, 1795.

24 W. Qiu, X. Xie, J. Qiu, W. Fang, R. Liang, X. Ren, X. Ji, G. Cui, A. M. Asiri, G. Cui, B. Tang and X. Sun, *Nat. Commun.*, 2018, **9**, 3485.